International Journal of Robotics and Automation, Vol. 36, 2021

Special Issue: Automatic Detection and Assessment of Bridge Structures

ANALYSIS OF INFLUENCE FACTORS FOR CFST ARCH BRIDGE VOID BASED ON EDDY CURRENT THERMAL IMAGING

Xiaokun Guo* and Heng Yan**

Abstract

Based on the principle of eddy current thermal imaging, a void detection test for concrete-filled steel tube (CFST) specimens was performed. The effects of the void thickness, steel tube wall thickness, heating power, and heating time were analysed experimentally. A model relating the heating rate and the influence factors was established to determine the sensitivity of the heating rate to the influence factors with multiple linear regression analysis. The following results are obtained: (1) The heating rate had positive linear relationships with the stripping thickness and heating power, and the heating rate had a negative linear correlation with the wall thickness. (2) An equation relating the heating rate with the stripping thickness, steel tube wall thickness, heating power, and heating time was obtained. The steel tube wall thickness and the heating power had the greatest influence on the heating rate. The results of this study can promote the application of eddy current thermal imaging technology and provide support for the development of void detection technology of CFST arch bridges.

Key Words

Eddy current thermal imaging, CFST, void detection, influence factors

1. Introduction

The concrete-filled steel tube (CFST) arch bridges are formed by steel pipes filled with concrete. This type of structure integrates the advantages of the two materials and has a strong bending resistance and high compressive strength [1]–[3]. Based on these advantages, CFST arch bridges are becoming more and more widely used. During actual use, due to factors, such as inadequate construction technology, large changes in the ambient temperature, and shrinkage and creep of the concrete, void defects appear in CFST arch bridges. These void defects adversely affect the force distribution across the entire bridge, and they can significantly affect the carrying capacity and constrain the service life of the CFST arch bridge [4]–[6].

At present, the research on the voiding of CFST arch bridges has mainly focused on the causes of the void age of the CFST, the detection of voids, the analysis of the mechanical properties after voiding, and preventive measures for voids. A variety of effective methods for detecting the voids of CFST arch bridges have been explored. The existing detection methods can be divided into two categories: non-destructive testing and destructive testing. Destructive testing is not commonly used because it requires the sampling of damaged steel cores and causes local damage to the structure. The non-destructive testing techniques for the void detection of CFST arch bridges mainly include ultrasonic methods [7], [8], optical fibre sensor measurements [9], [10], impact elastic wave methods [11], [12], and infrared thermal imaging methods [13]–[15].

Pulsed eddy current thermography [16]–[18] is a type of infrared thermography. In this method, the test piece is heated by a transient pulse. The temperature distribution on the surface of the test piece is obtained, and the region where the temperature is abnormal is extracted. The defect is thereby detected. Compared with the traditional infrared thermal imaging method, the method has the advantages of a fast heating speed, controllable heating rate, and simple quantification of the degree of voiding.

At present, researchers worldwide have conducted a series of studies on eddy current thermal imaging. Li *et al.* [19] proposed a complete strategy to perform pre- and post-processing for surface crack detection based on the eddy current pulsed thermography (ECPT) platform. In addition, quantitative evaluation was involved to objectively evaluate detectability. In particular, a new post-image segmentation algorithm was proposed based on the idea of grouping histograms and iterative adaption approaches, which leads to better performance for quantitatively identifying and sizing the defect. Shi *et al.* [20] applied ECPT for quantitative crack detection based on derivative analysis of the temperature variations. The crack contours and positions in a hot image were detected and analysed,

* Southwest Transportation Construction Group Co., Ltd., Kunming 650501, P.R. China; e-mail: guoxiaokun1234@163.com

** YCIC Highway Construction Fifth Engineering Co., Ltd., Kunming 650228, P.R. China; e-mail: 410282160@qq.com

Corresponding author: Xiaokun Guo

Recommended by Dr. Jingzhou Xin

(DOI: 10.2316/J.2021.206-0543)

and the results showed that this method could detect the crack size quantitatively with small errors. He *et al.* [21] proposed two methods to suppress the influence of the non-uniform emissivity in eddy current thermal imaging. Liu *et al.* [22] studied the influence of the thermal imaging sampling rate on defect feature extraction. Different thermal imaging sampling rates were used for different characterizations. Based on the robustness of different sampling rates, corresponding sampling rates were obtained.

However, eddy current thermal imaging methods are rarely applied for void detection of CFST arch bridges, and thus this subject needs further research. In addition, many factors, such as the defect thickness and steel tube wall thickness, will have impacts on the detection results in the actual eddy current thermal imaging stripping detection process. However, research and analysis on these influence factors are lacking. Based on the principle of eddy current thermal imaging, a void detection test of CFST specimens was examined in this study. Factors, such as the defect width, steel tube wall thickness, heating power, and heating time, were analysed experimentally to determine their influence on the detection effect.

2. Principle

The induction heating of steel tubes is actually due to magnetic induction generated in the conductor by electromagnetic induction, and an eddy current is generated to heat the workpiece. It relies on an induction coil to transmit electrical energy through electromagnetic induction to the heated metal, where the resulting joule heat is stored, raising the temperature of the metal. To illustrate this effect, the heating process of a cylindrical metal workpiece is shown in Fig. 1. When the spiral induction coil passes through the alternating current, the alternating magnetic field reverses. When the magnetic field lines pass through and return to the metal workpiece, a closed loop is formed, and the cross section of the metal generates an induced current called an eddy current.

The detailed principle of electromagnetic induction heating can be explained by the electromagnetic induction and Joule–Lenz (JL) theorems. The electromagnetic induction theorem states that when a closed loop passes through an alternating current, the generated magnetic flux crosses the surface formed by the closed loop. The magnitude of the magnetic flux value changes with time, and the induced electromotive force forms in the closed loop. This is expressed as follows:

$$e = d\phi/dt \tag{1}$$

where e is induction electromotive force, ϕ is magnetic flux, and t is time.

Due to the electromotive force generated in the workpiece and the resistance in the workpiece, the joule heat is generated by the eddy current. The joule heat can be expressed by the JL theorem:

$$Q = I^2Rt \tag{2}$$

where Q is heat, I is the current flowing through the conductor, R is the resistance of the conductor, and t is heating time.

The induction heating process consists of two processes. One is the process in which the electromagnetic induction generates an induced electromotive force to generate joule heat, and the other is the heat conduction process in the workpiece. The distribution and size of the electromotive force generated in the former process play leading roles in the heat conduction in the latter process. According to the principle of thermodynamics, the amount of heat can be obtained by multiplying the power and heating time as follows:

$$Q = Pt \tag{3}$$

where P is heating power.

The heating power is determined by the current and resistance together, which can be expressed as follows:

$$P = I^2R \tag{4}$$

For induction heating, the induced power in the detected workpiece is expressed approximately as follows:

$$P = I^2_{\text{inductor}}\sqrt{\mu f/\sigma}. \tag{5}$$

Equation (5) can be substituted into (3) to obtain the heat generated by the eddy current as follows:

$$Q = tI^2_{\text{inductor}}\sqrt{\mu f/\sigma} \tag{6}$$

where t is the heating time, I_{inductor} is the current in the induction coil (excitation current), f is the frequency of the excitation current, μ is the material permeability, and σ is the conductivity of the material. Induction heating is related to the amplitude of the excitation current, the frequency of the excitation current, the heating time, the conductivity, and the permeability of the tested material.

For CFST arch bridges, there are generally different degrees of void detection. The hollower the CFST is, the slower the heat transfer from the surface of the CFST to

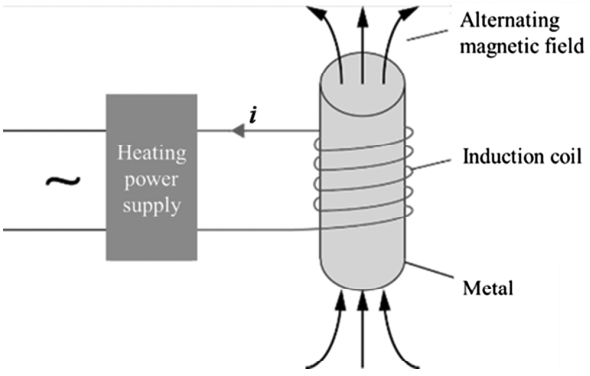

Figure 1. Schematic of the electromagnetic induction heating process.

Table 1
Sizes of Specimens (mm)

Number	Specimen Size (Height × Diameter × Wall Thickness)	Defect Size (Length × Width × Height)	Note
1	300 × 160 × 2	100 × 50 × 5	Defect sizes varied
2	300 × 160 × 2	100 × 50 × 10	
3	300 × 160 × 2	100 × 50 × 15	
4	300 × 160 × 2	100 × 50 × 20	
5	300 × 160 × 2	20 × 50 × 10	
	300 × 160 × 2	50 × 50 × 10	
6	300 × 160 × 5	100 × 50 × 10	Steel tube wall thickness varied
7	300 × 160 × 10	100 × 50 × 10	

the internal concrete will be, and the faster the surface temperature of the CFST will rise when the CFST is heated. Therefore, the void quantity of the CFST can be determined by measuring the rate of surface temperature increase during the heating process of the CFST. Pulsed eddy current induction heating is an efficient heating method, which can rapidly heat a specimen.

3. Experiment

3.1 Experiment Preparation

Based on engineering practice, a CFST gradually forms voids under the influence of a temperature load, concrete shrinkage and creep, and construction influences. The thermal conductivity of air is 0.023. To better simulate the actual process, polyacetylene plastic foam, which is lightweight and has a thermal conductivity close to that of air, was selected as the filling material for comparison. The foam was prepasted on the inner walls of the steel tube to simulate the void defect.

To prepare the specimens, the filling material was laid in advance to simulate the void, and the strength of the poured concrete was selected as C30. The inner diameter and height of the steel pipe ring were 16 cm and 30 cm, respectively. To study the effects of external factors (*e.g.*, heating time and driving power) and internal factors (*e.g.*, steel tube wall thickness and thickness of pavement) on the concrete surface temperature change, the influence factors of the heating rate and the sensitivity of factors were analysed. To determine the positions and sizes of the defects, the defect sizes were 100 mm × 50 mm, 50 mm × 50 mm, and 20 mm × 50 mm. The void thicknesses were 0, 5, 10, 15, and 20 mm. These defects were arranged at the centre of the steel tube, and the detailed sizes of the specimens are shown in Table 1.

The main pieces of equipment used in the test process included a power supply, eddy current heating device, infrared thermal imager, and information processing system. The power supply was a common 220 V AC power supply. The pulsed eddy current heating device produced by Hubei Zhongyuan Electronic Equipment Company included two components: a heating device and a cooling device. The output power, the frequency variation range, and the output current of the heating device were 15 kW, 30–100 kHz, and 200–600 A, respectively. The infrared camera was a model A310, produced by the FLIR Company of the United States. Using an infrared camera allowed temperature measurements to be obtained economically and accurately by a user using a computer, with a detection accuracy of 0.1°C. The information processing system could process the temperature data collected by the infrared camera from the surfaces of the specimens. The processing included the preprocessing of the collected signals, the analysis and calibration of the influence factors, the display of the measurement results, and the querying of the previous parameter values. The entire detection system is shown in Fig. 2.

The experiments explored the factors that affected the surface heating rate during the heating process of the CFST specimens to provide guidance for the realization of accurate void detection technology. Therefore, the CFST was placed under an induction heating coil for heating, and

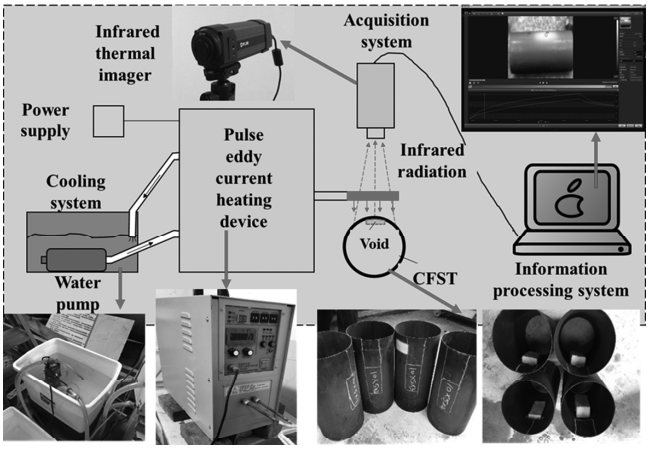

Figure 2. Eddy current thermal imaging void of concrete-filled steel tube detection system.

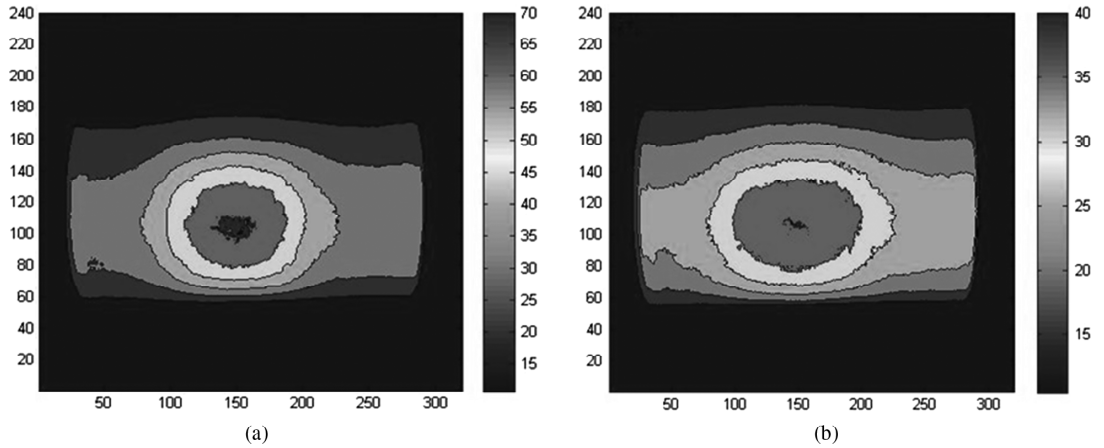

Figure 3. Temperature cloud after heating the steel pipe: (a) temperature rise stage and (b) temperature drop stage.

the temperature variation of the surface of the test piece was obtained. This process was as follows.

1. The rust and concrete on the surface of the test piece were removed with sand paper to prevent the impurities on the surface of the test piece from affecting the test results. The surface of the specimen to facilitate heating and positioning was marked.
2. The infrared thermal imager and information processing system were installed and debugged, and the environmental parameters were fixed.
3. The lift height of the coil was adjusted by changing the height of the mat to the centre of the spiral coil.
4. After the above preparations were complete, the cooling circulation system was started. The induction heating device was precooled and kept at a low temperature to ensure that it was not to be damaged by high temperatures.
5. The infrared thermal imager acquisition button was opened in advance to collect the surface temperature data of the test piece. The instrument power supply was turned on, and the eddy current heating time was set. In addition, the heating power was turn on, and the specimen was heated.
6. After the specified heating time, the induction heating device automatically stopped heating and simultaneously removed the coil. After the surface temperature of the specimen was lowered to room temperature, the thermal imager recording was stopped.

3.2 Experimental Results

The temperature measurement point was marked on the centres of the surfaces of the hollow sections of the CFST specimens, denoted as point A. This point was located directly below the induction heating coil to ensure that the relative positions of the CFST specimens and the induction coil did not change during induction heating.

The CFST specimens were placed directly under the induction coil. Under the excitation of the high-frequency alternating magnetic flux, the steel pipe directly under the coil induced a current (eddy current) to generate joule heat. Therefore, the surface temperatures of the CFSTs increased rapidly. Since the internal heat balance of the CFST was broken, heat was transferred from the surface of the high-temperature steel pipe to the concrete with a low internal temperature, which caused the surface temperature of the concrete-filled steel-pipe specimen to change. The infrared thermal imager was used to collect the surface temperature data during the induction heating and cooling of the test piece. The infrared thermal image cloud of the surface temperature rise of the test piece is shown in Fig. 3(a). The temperature reduction stage is shown in Fig. 3(b), where brighter regions correspond to higher temperatures.

Figure 3 shows that after the induction heating began, the surface temperature of the CFST immediately below the spiral coil increased rapidly. With the increase in the cooling time and transfer of the heat to the core concrete of the steel pipe transversely and internally, the surface temperatures of the CFST specimens continuously decreased, and the temperature isotherms became elliptical.

To further study the variation of the temperature in the experiment, the temperature data at measurement point A in the induction heating and cooling processes were extracted. The time–temperature data at this point were plotted as shown in Fig. 4.

As shown in Fig. 4, after the induction heating began, the temperature at point A increased rapidly. When the specified heating time was reached, the power was turned off to stop the heating, and the coil was removed. According to the principle of induction heating, the temperature of the steel pipe increased rapidly after being excited by the eddy current. However, the temperature did not decrease immediately after removing the heating coil. The reason for this was that after the induction coil was removed, the surface temperature of the steel pipe continued to rise due to the residual eddy current. After the residual eddy current disappeared, the maximum temperature was reached, and the cooling stage began. In the induction heating and cooling stage of the CFST, the temperature of the steel pipe was higher than the internal concrete. The heat was transmitted along the longitudinal direction of the steel

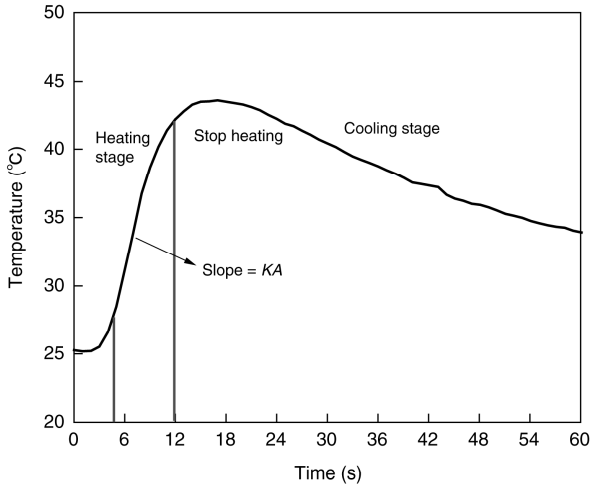

Figure 4. Variations in the temperature of the test piece at measurement point A with time.

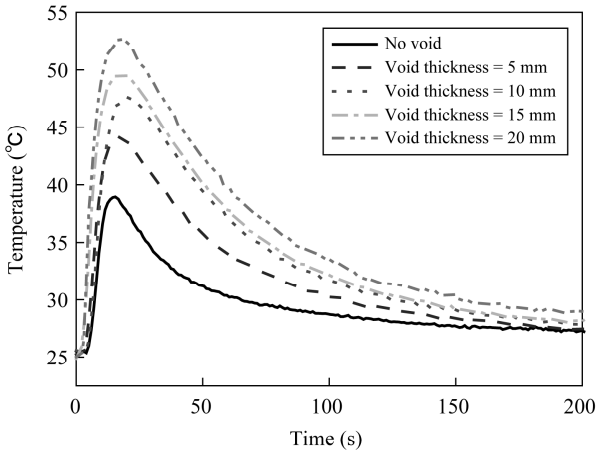

Figure 5. Variations in the surface temperatures of the concrete-filled steel tubes with time for different void thicknesses.

pipe and the concrete. Due to the presence of the void, the surface heating and cooling rates of the CFST specimens were different.

The temperature rise could be controlled by changing parameters such as the power, and the heating time was short. The cooling process occurred through natural conduction and heat dissipation via convection. Thus, the surrounding environment had a great influence on the detection result. Therefore, the heating rate, as the characteristic parameter, was used to analyse the influence factors.

3.3 Analysis of Influence Factors

3.3.1 Effect of Depth Thickness on Temperature Rise Rate of Concrete-filled Steel Tube Surface

To investigate the effect of the CFST thickness on the rates of surface temperature increase of the CFST specimens, specimens No. 1–4 (thicknesses of the voids were 5, 10, 15, and 20 mm, respectively) were tested. The experiment used the control variable method. Therefore, the other parameters of the instrument were constant during the tests. The heating power, input current, frequency, coil lift height, and eddy current heating time were set to 3 kW, 200 A, 60 kHz, 2 cm, and 6 s, respectively. The temperature data collected by the infrared camera were plotted, and the variations in the surface temperature of the CFST with time for different void thicknesses were obtained as shown in Fig. 5.

Figure 5 shows that the surface temperatures of the CFST specimens with different void thicknesses varied with time. During the induction heating process, the surface temperature of the test piece increased rapidly, and the heating rate reached 3°C/s. With the increase in the void thickness for the different CFST specimens, the maximum surface temperature and rate of temperature rise also increased. To further analyse the effect of the thickness of the void on the rate of temperature rise, the temperature increase of the CFST during the heating process was fitted to obtain the rate of temperature rise of the surface of the CFST (the slope of the fitted curve in Fig. 5) as shown in Fig. 6.

As shown in Fig. 6, for different void thicknesses, the surface temperature rise rates of the CFST specimens were different. The greater the void thickness was, the higher the surface heating rate of the CFST specimens became. With the increase in heating time, the temperature at point A increased almost linearly for different void thicknesses. The R^2 (coefficient of determination) values, representing the goodness of fit, were all greater than 0.97, indicating that the data were fit well by linear models. However, the slopes of the fitting curves were different, indicating that the thickness of the void affected the heat conduction. Furthermore, the different void thicknesses and the heating rate were plotted together, and the results were shown in Fig. 6(b). The heating rate increased linearly with the void thickness. The greater the void thickness was, the greater the heating rate became. The linear relationship between the heating rate and the thickness of the void, which was obtained by a linear fit, was expressed as follows:

$$Y = 1.7078X_1 + 0.09088 \tag{7}$$

where Y represents CFST surface heating rate (°C/s) and X_1 represents the void thickness (mm).

3.3.2 Effect of Wall Thickness of Steel Tubes on the Concrete-filled Steel Tube Surface Temperature Rise Rate

To investigate the influence of the wall thickness on the surface temperature rise rate of the CFST specimens, specimens No. 2, 6, and 7 (wall thicknesses of 2, 5, and 10 mm, respectively) were selected as test objects. To prevent the influence of other factors, the detection parameters were the same as those in the previous experiments. The temperature data collected by the infrared camera were plotted for different wall thicknesses as shown in Fig. 7.

As shown in Fig. 7(a), as the wall thickness of the steel pipe decreased, the temperature–time curves of the

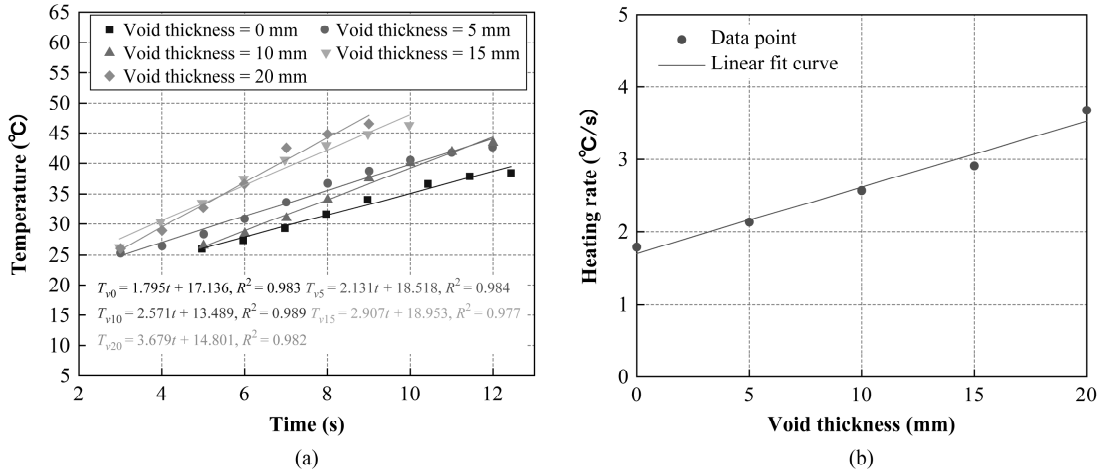

Figure 6. Heating rates for different void thicknesses were analysed: (a) time-dependent diagram of the surface temperature of the CFST specimens during heating for different void thicknesses and (b) relationship between the void thickness and heating rate.

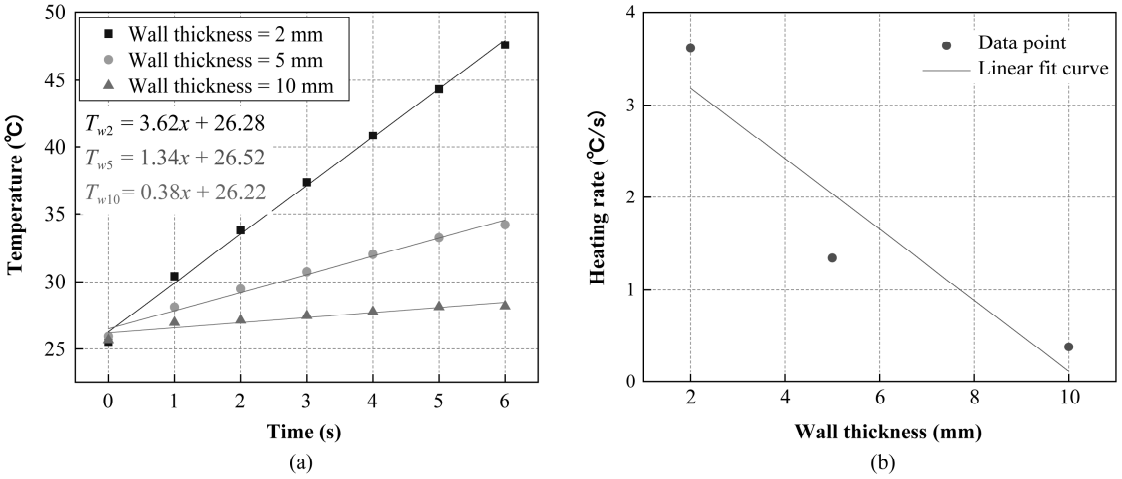

Figure 7. Heating rates of the steel tube for various wall thicknesses were analysed: (a) time-dependent surface temperatures of the concrete-filled steel tubes for different wall thicknesses and (b) relationship between the steel tube wall thickness and the heating rate.

surface of the CFST gradually became steeper. The reason for this was that the steel pipe was a material with a relatively uniform texture, and it underwent a linear change during the heating process. It shows that the heating rate of the surface temperature of the CFST was inversely proportional to the wall thickness of the steel pipe. The reason for this phenomenon was that a thicker wall of the steel pipe corresponded to a greater amount of heat that could be absorbed at the measurement point. Therefore, in Fig. 7, the slope of the curve was smaller. The linear relationship between the heating rate and the thickness of the steel tube wall, which was obtained by a linear fit, was expressed as follows:

$$Y = -0.38327X_2 + 3.95184 \tag{8}$$

where Y is the heating rate of the CFST surface (°C/s) and X_2 is the steel pipe wall thickness (mm).

3.3.3 Effect of Heating Power on Concrete-filled Steel Tube Surface Temperature Rise Rate

To investigate the influence of the eddy current heating power on the surface temperature rise rate of the CFST specimens, the test piece No. 3 was selected as the test object. The heating powers of the instrument were P1, P2, P3, and P4 (2, 3, 4, and 5 kW, respectively). The remaining detection parameters were unchanged. The variations in the surface temperature of the CFST with time for different heating powers are shown in Fig. 8.

As shown in Fig. 8, the surface temperatures of the CFST specimens increased continuously with the increase in the eddy current heating power after the same heating time. During the temperature rise stage, the greater the eddy current heating power was, the steeper the surface temperature growth curve of the CFST specimen became. To further explore the relationship between the heating rate of the parameters and the heating power, the

temperature rising processes were discussed separately. As shown in Fig. 8, during the heating process, the temperature increased almost linearly with time. Therefore, the surface temperature data of the CFST were linearly fitted during the heating process, and the slope of the fitting result was the temperature rise rate, as shown in Fig. 9(a).

For different heating powers, the surface temperature rise rates of the CFST specimens were different, as shown in Fig. 9(a). The higher the eddy current heating power was, the higher the surface heating rate of the CFST specimens became. The different heating powers were plotted with their heating rates, and the data points were linearly fitted. The fitting results are shown in Fig. 9(b), and the fit equation was expressed as follows:

$$Y = 0.6106X_3 - 0.0726 \tag{9}$$

where Y represents the CFST surface heating rate (°C/s) and X_3 is the heating power (kW).

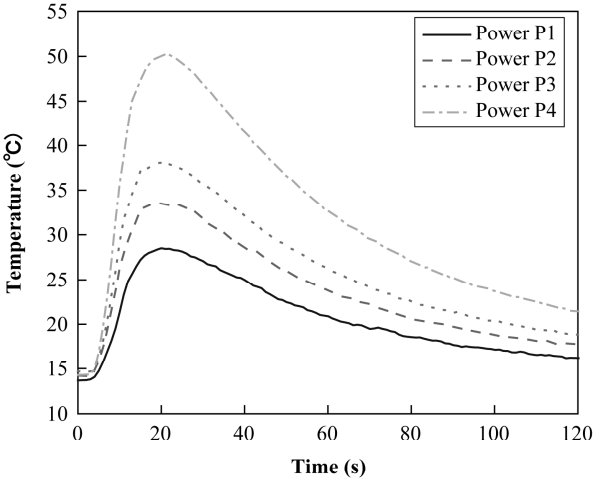

Figure 8. Variations in the surface temperatures of the concrete-filled steel tubes with time for different heating powers.

Figure 9(b) shows that the rate of temperature increase of the CSFT increased as the heating power increased. The slope in (9) is significantly smaller than that in (7), indicating that the heating power has a smaller influence on the heating rate than the void thickness.

3.3.4 Effect of Different Heating Time on Temperature Rise Rate of Concrete-filled Steel Tube Surface

Test piece No. 1 was selected as the test object, and the heating time of the instrument were $t1$, $t2$, $t3$, and $t4$ (3, 6, 10, and 15 s, respectively). The other parameters were not changed. The power of the high-frequency induction heater was 3 kW, the current in the induction coil was 200 A, the frequency was about 60 kHz, and the coil lift-off height was 2 cm. The results are shown in Fig. 10.

As shown in Fig. 10(a), the longer the heating time was in the temperature rising stage, the higher the maximum surface temperatures of the CFST specimens were. However, under different heating time, the surface temperature rise trends of the test pieces were basically the same. The data from the temperature rise stage of the CFST specimens in Fig. 10 were linearly fitted, and the surface temperature rise rates of the CFST specimens after different heating time were obtained as shown in Fig. 10(b). The curve in Fig. 10(b) varied slowly, which indicated that the eddy current heating time did not significantly affect the surface temperature rise rate of the CFST. To quantify the relationship between the heating rate and the heating time, a linear fit of the two relationships is shown in (10):

$$Y = 0.01315X_4 + 3.08074 \tag{10}$$

where Y represents CFST surface heating rate (°C/s) and X_4 represents the heating time (s).

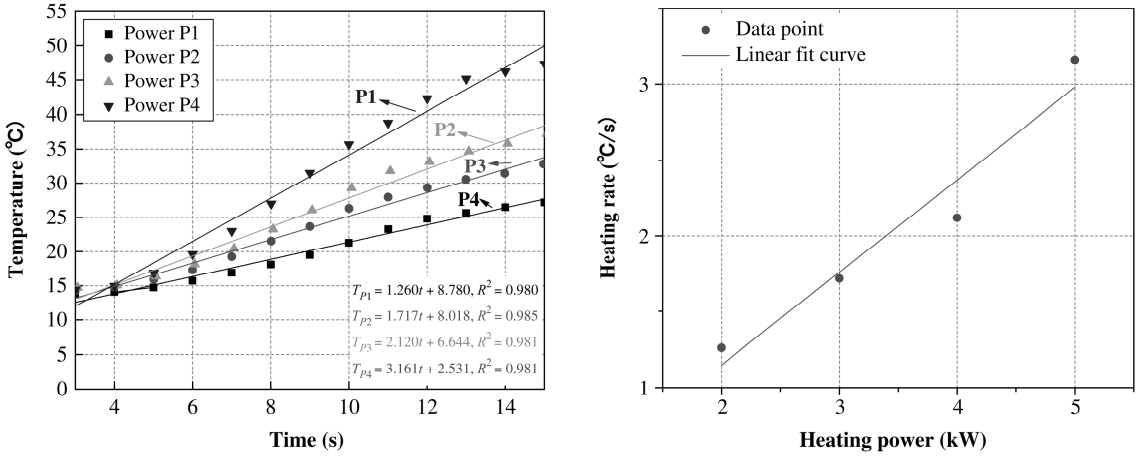

Figure 9. Temperatures and heating rates at different heating powers during the heating stage: (a) time-dependent surface temperatures of the CFST specimens during heating for different heating powers and (b) relationship between the surface heating rate and the heating power of CFST specimens.

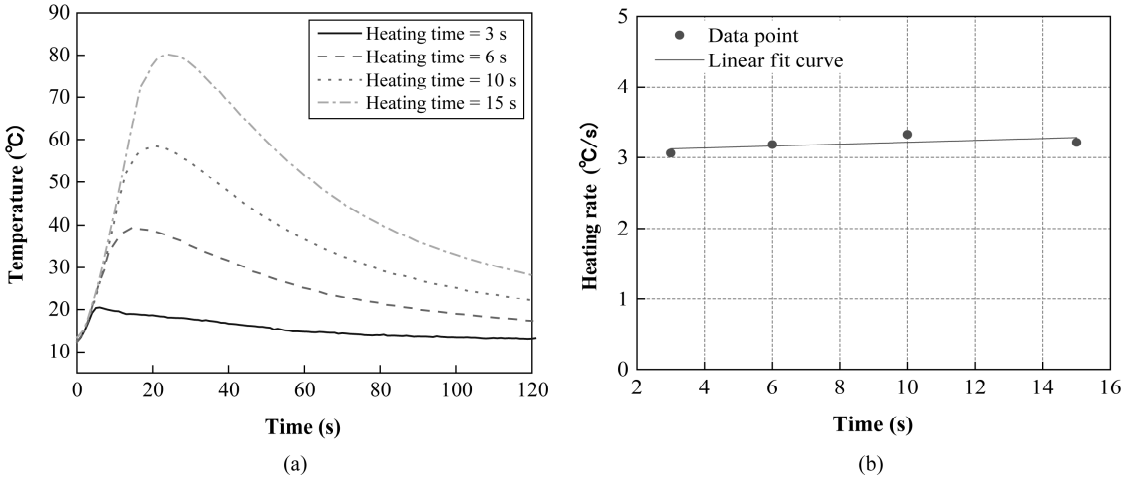

Figure 10. Effect of the heating time on the heating rate: (a) variations of the surface temperature of the concrete-filled steel tubes with time for different heating times and (b) relationship between the surface heating rate and the heating time of the CFST specimens.

Table 2
Concrete Tube Concrete Surface Temperature Heating Rate Regression Data

Number	X_1 (mm)	X_2 (mm)	X_3 (kW)	X_4 (s)	Y(°C/s)	Number	X_1 (mm)	X_2 (mm)	X_3 (kW)	X_4 (s)	Y(°C/s)
1	0	2	3	6	1.8	9	15	2	2	6	1.3
2	5	2	3	6	2.1	10	15	2	3	6	1.7
3	10	2	3	6	2.6	11	15	2	4	6	2.1
4	15	2	3	6	2.9	12	15	2	5	6	3.2
5	20	2	3	6	3.7	13	5	2	3	3	2.1
6	10	2	3	6	3.6	14	5	2	3	6	2.2
7	10	5	3	6	1.3	15	5	2	3	10	2.2
8	10	10	3	6	0.4	16	5	2	3	15	2.2

3.4 Multifactor Sensitivity Analysis

Based on the earlier analysis, the surface temperature rise rate of the CFST was influenced by several factors. In an actual project, the influence factors do not exist in isolation, but multiple factors are present simultaneously. Thus, it is very important to study the influence of multiple factors on the heating rate. To study the sensitivity of the temperature rise rate of the CFST to different influence factors, a simple model relating them was established and analysed using a multiple linear regression. The void thickness X_1, the wall thickness X_2, the heating power X_3, and the heating time X_4 were selected as the independent variables. The surface heating rate Y of the CFST was used as the response variable for the multiple linear regression analysis. The regression analysis data are shown in Table 2.

The regression equations were different depending on the number of independent variables included. The number of elements of the multiple regression equation was the same as the number of independent variables. In this study, four independent variables were used to establish a quaternary linear regression equation. The results are shown as follows:

$$Y = 1.38 + 0.04X_1 - 0.26X_2 + 0.35X_3 + 0.005X_4 \quad (11)$$

where Y denotes the CFST surface heating rate (°C/s), X_1 denotes the void thickness (mm), X_2 denotes the steel pipe wall thickness (mm), X_3 denotes the heating power (kW), and X_4 denotes the heating time (s).

The regression coefficients obtained by multiple regression were different from those obtained during the single-factor analysis because the single-factor analysis can represent only a simple correspondence. A multiple linear regression considers the combined effects of multiple influence factors on the heating rate.

The following can be determined from (11). Among the four influence factors, the regression coefficient of the

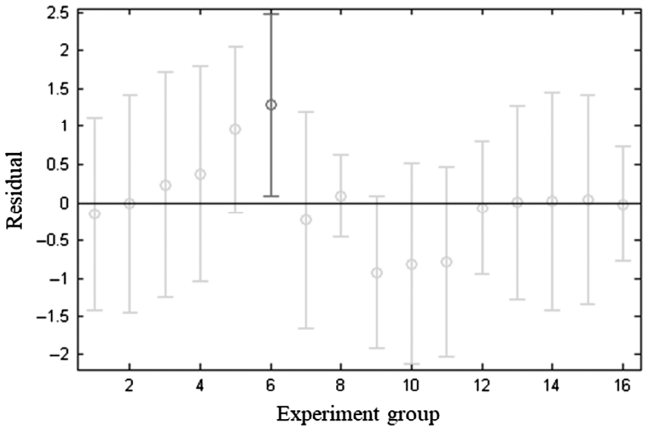

Figure 11. Residual calculation result.

heating power X_3 was the largest positive coefficient, indicating that the heating rate was most sensitive to the heating power. The regression coefficient of the wall thickness X_2 of the steel pipe was the largest negative coefficient. Thus, the increase in the wall thickness of the surface steel pipe led to a decrease of the heating rate, which is consistent with the analysis presented earlier. The regression coefficient of the heating time X_4 was the smallest, with a value less than 0.01, and the heating rate was not sensitive to the heating time. The regression coefficient of the void thickness X_1 was 0.04, which showed that the void thickness had a certain influence on the heating rate, but the degree of influence was smaller than those of X_2 and X_3. The regression equation results were consistent with the data, indicating that the regression model was reasonable. To test the difference between the regression model obtained from the sample and the population, an F test was performed on the regression model. The probability of sampling error of the F test (P value) was 0.0004 ($P < 0.001$), indicating that the fitting model was valid and statistically significant. The residuals were calculated, and the results were shown in Fig. 11. One set of data deviated from the residual of 0 (shown in thick line in Fig. 11), and the rest were distributed around 0, indicating that the model had a good fitting effect.

As known from the above analysis, the surface temperature rise rate of the CFST was sensitive to different influence factors. When the heating parameters (*e.g.*, power and time) were fixed, the influence of the wall thickness of the steel pipe was much greater than the thickness of the void. Therefore, in an actual testing process, the influence of the wall thickness of the steel pipe should be considered.

4. Conclusion

By examining the CFST, the following conclusions were drawn:

1. Through eddy current heating tests for CFST, the surface temperature rises of the CFST specimens were stable and rapid during the heating stage. The heating rate in the heating stage is an important parameter for analysing the effect of void for CFST.
2. Analysis of the factors that affected the void detection, such as the thickness of the void, the wall thickness of the steel pipe, the heating power, and the heating time, showed that the heating rate was positively linearly related to the thickness of the void and the heating power. The heating rate was negatively linearly related to the wall thickness. The heating time had almost no effect on the heating rate.
3. Through the multiple linear regression analysis method, the relationship between the heating rate and the void thickness, steel tube wall thickness, heating power, and heating time was established. The wall thickness and heating power of the steel tube had the greatest influence on the heating rate. In an actual test for determining the heating power and heating time, the influence of the thickness of the steel pipe on the detection should be fully considered.
4. Based on the theory of eddy current thermal imaging, the influence factors of the CFST void detection process were analysed. The results of this study clearly identified the significance of the influence factors for engineering applications. This approach improves upon the existing method of void detection that is typically used for the CFST.

Acknowledgement

This research was financially supported by the Science and Technology Project of Yunnan Provincial Transportation Department (No. [2018]27).

References

[1] B.C. Chen, J.G. Wei, J. Zhou, *et al.*, Application of concrete-filled steel tube arch bridges in China: Current status and prospects, *China Civil Engineering Journal, 50*(6), 2017, 54–65.

[2] R. Yadav, B. Chen, H. Yuan, *et al.*, Experimental investigation of CFST-RC bridge piers under cyclic loading, *Procedia Engineering, 173*, 2017, 1723–1730.

[3] S. Rajeev, D. John Peter, and M.V. Varkey, Study of concrete filled steel tubular arch bridge: A review, *Applied Mechanics & Materials, 857*, 2017, 261–266.

[4] J. Zhang, Y. Li, G.F. Du, *et al.*, Damage detection of L-shaped concrete filled steel tube (L-CFST) columns under cyclic loading using embedded piezoceramic transducers, *Sensors, 18*(7), 2018, 2171–2192.

[5] A.L. Krishan, E.P. Chernyshova, and R.R. Rustam, The bearing capacity of the pre-compressed concrete filled steel tube columns, *Defect & Diffusion Forum, 382*, 2018, 261–266.

[6] M.Y. Liu and W.G. Yuan, Research on safety assessment of long-span concrete-filled steel tube arch bridge based on fuzzy-neural network, *China Journal of Highway and Transport, 17*(4), 2004, 55–58.

[7] S.S. Shi and Q. Guan, Ultrasonic testing method of quantitative detection of flaws in concrete filled steel tube, *Nondestructive Testing, 33*(3), 2011, 66–72.

[8] Y.F. Xiao, Approach of concrete-filled steel tube ultrasonic method based on ANN, *Applied Mechanics & Materials, 105–107*, 2012, 1611–1615.

[9] G.F. Du, Z. Li, and G.B. Song, A PVDF-based sensor for internal stress monitoring of a concrete-filled steel tubular (CFST) column subject to impact loads, *Sensors, 18*(6), 2018, 1682.

[10] Y. Bao, M.S. Hoehler, C.M. Smith, *et al.* Temperature measurement and damage detection in concrete beams exposed

to fire using PPP-BOTDA based fiber optic sensors, *Smart Materials & Structures, 26*(10), 2017, 1–32.
[11] A.Z. Zhu, W. Xu, K. Gao, *et al.*, Lateral impact response of rectangular hollow and partially concrete-filled steel tubular columns, *Thin-Walled Structures, 130*, 2018, 114–131.
[12] H.Z. Wang, Analytical solution for stress waves of hollow concrete filled steel tubular piles subjected to axial impact, *Engineering Mechanics*, *4*, 2017, 106–112.
[13] R. Xu, D.H. Jiang, and X.W. Lu, Research on the application of the infrared thermal image method in detection of concrete density of concrete-filled steel tube, *Applied Mechanics & Materials, 166–169*, 2012, 998–1001.
[14] Q. Liu and H. Zhou, Research on density detection method of rock-filled concrete by infrared imaging technology, *Industrial Construction, 41*(3), 2011, 113–112.
[15] L. Cheng and G.Y. Tian, Surface crack detection for carbon fiber reinforced plastic (CFRP) materials using pulsed eddy current thermography, *IEEE Sensors Journal, 11*(12), 2011, 3261–3268.
[16] Z.P. Liu, G. Lu, X.L. Liu, *et al.*, Image processing algorithms for crack detection in welded structures via pulsed eddy current thermal imaging, *IEEE Instrumentation & Measurement Magazine, 20*(4), 2017, 34–44.
[17] Q.L. Jin, D.X. Hou, Z.Q. Jin, *et al.*, A fast frequency tracking algorithm for pulsed eddy current thermal imaging power supply, *Power Electronics, 48*(12), 2014, 3.
[18] L. Liu, D. Zheng, J.T. Zhou, *et al.* Corrosion detection of bridge reinforced concrete with induction heating and infrared thermography, *International Journal of Robotics and Automation, 33*(4), 2018, 379–385.
[19] X.Q. Li, B. Gao, W.L. Woo, *et al.*, Quantitative surface crack evaluation based on eddy current pulsed thermography, *IEEE Sensors Journal, 17*(2), 2017, 412–421.
[20] Z.Q. Shi, X.Y. Xu, J.J. Ma, *et al.*, Quantitative detection of cracks in steel using eddy current pulsed thermography, *Sensors, 18*(4), 2018, 1070.
[21] M. He, L.B. Zhang, J.Y. Li, *et al.*, Methods for suppression of the effect of uneven surface emissivity of material in the moving mode of eddy current thermography, *Applied Thermal Engineering, 118*, 2017, 612–620.
[22] J. Liu, G.Y. Tian, B. Gao, *et al.*, Investigation of thermal imaging sampling frequency for eddy current pulsed thermography, *NDT & E International, 62*(2) 2014, 85–92.

Biographies

Xiaokun Guo was born in April 1977, Lu Liang, Yunnan and belongs to Han nationality. He is the member of the Communist Party of China. He received his bachelor degree in engineering. He is a Senior Engineer and a First-level Construction Engineer of highway engineering. He is working in Southwest Transportation Construction Group Co., Ltd, Kunming, China. His research interests are the bridge non-destructive testing and the health monitoring.

Heng Yan graduated from Chongqing Jiaotong University. He is working in YCIC Highway Construction Fifth Engineering Co., Ltd, Kunming, China. His research interest is the bridge non-destructive testing.